

1 **Title: STK25 inhibits PKA signaling by phosphorylating PRKAR1A**

2 **Authors:** Xiaokan Zhang¹, Bryan Z. Wang^{1,2}, Michael Kim¹, Trevor R. Nash^{1,2}, Bohao Liu^{1,2}, Jenny
3 Rao¹, Roberta Lock², Manuel Tamargo², Rajesh Kumar Soni³, John Belov¹, Eric Li¹, Gordana
4 Vunjak-Novakovic^{1,2} and Barry Fine^{1*}

5
6 **Affiliations**

7 ¹ Department of Medicine, Division of Cardiology, Columbia University Irving Medical Center, New
8 York, NY, USA

9 ² Department of Biomedical Engineering, Columbia University, New York, NY, USA

10 ³ Proteomics and Macromolecular Crystallography Shared Resource, Herbert Irving
11 Comprehensive Cancer Center, Columbia University Irving Medical Center, New York, NY, USA

12

13 ***Corresponding Author**

14 Barry Fine MD PhD

15 Department of Medicine, Division of Cardiology

16 622 West 168th Street

17 PH8-405B

18 New York, NY 10032

19

20 **Preprint Server: bioRxiv, 2022.01.27.478084**

21

22

23 **Keywords:** STK25, PRKAR1A, Protein Kinase A, induced pluripotent stem cell

24

1 **Summary**

2 In the heart, Protein Kinase A (PKA) is critical for activating calcium handling and sarcomeric
3 proteins in response to beta adrenergic stimulation leading to increased myocardial contractility
4 and performance. The catalytic activity of PKA is tightly regulated by regulatory subunits which
5 inhibit the catalytic subunit until released by cAMP binding. Phosphorylation of Type II regulatory
6 subunits promotes PKA activation, however the role of phosphorylation in Type I regulatory
7 subunits remain uncertain. Here we utilized human induced pluripotent stem cell cardiomyocytes
8 (iPSC-CM) to identify STK25 as a kinase of the Type I α regulatory subunit PRKAR1A.
9 Phosphorylation of PRKAR1A led to inhibition of PKA kinase activity and increased binding to the
10 catalytic subunit in the presence of cAMP. *Stk25* knockout in mice diminished *Prkar1a*
11 phosphorylation, increased *Pka* activity and augmented contractile response to beta adrenergic
12 stimulation. Together, these data support STK25 as a negative regulator of PKA signaling
13 through phosphorylation of PRKAR1A.

14

15

16

17

18

19

20

1 Introduction

2 Second messengers are key relays in the transduction of external cues into intracellular
3 signaling cascades. cAMP is a prototypical second messenger generated downstream from G
4 protein coupled receptors and is involved in integrating a diverse set of signaling pathways
5 (Gancedo, 2013). The classic and most widely studied effector of cAMP is PKA and it has been
6 broadly implicated in a diverse set of cellular processes including the cell cycle, proliferation,
7 cytoskeletal dynamics, ion flux and beta adrenergic signaling (Tasken and Aandahl, 2004; Taylor
8 et al., 2012). Specificity of signaling in a system with such a broad set of substrates relies on
9 careful regulation of both cAMP metabolism as well as compartmentalization of PKA through a
10 series of A kinase anchoring proteins (AKAP) (Colledge and Scott, 1999). These AKAPs bind to
11 the regulatory subunits of PKA and direct its activity to a discrete set of effectors and substrates,
12 thereby allowing for enhanced spatiotemporal control over PKA and the pathways it activates.

13 The PKA holoenzyme is comprised of a regulatory subunit dimer and two catalytic units
14 (Kim et al., 2007). The main function of the regulatory subunit is to inactivate kinase activity in
15 the absence of cAMP. There are two classes of regulatory subunits, Type I and Type II, each
16 with an alpha and beta isoform. Binding of cAMP to the C terminal tandem cAMP binding domains
17 of the regulatory subunits releases the catalytic domain, allowing for kinase activity (Barradeau et
18 al., 2002). Type II regulatory subunits have a PKA substrate motif in the N -terminus (RRXS),
19 which is phosphorylated by the catalytic subunit upon binding to cAMP, enhancing its release and
20 activation (Taylor et al., 1990). They also are the primary target of AKAPs, binding at nanomolar
21 affinities (Colledge and Scott, 1999). The regulation of Type I subunits however remains less well
22 understood. They contain a pseudo-substrate (RRXxA/G) sequence that cannot be
23 phosphorylated by the catalytic subunit. Although phosphorylation of the Type I subunits has
24 been reported as part of large phosphoproteomic projects, their role in regulation of PKA activity
25 has not been demonstrated *in vivo* (Daub et al., 2008; Olsen et al., 2006; Olsen et al., 2010;
26 Oppermann et al., 2009; Zhou et al., 2013). Furthermore, the vast majority AKAP proteins do not

1 interact with Type I subunits, and the dual specificity AKAP proteins that do interact with Type I
2 subunits do so with significantly lower affinities compared to Type II subunits.

3 In the heart, PKA mediates beta adrenergic activation of the physiologic flight or fight
4 response, modulating both heart rate and myocardial contractility (Wang et al., 2018). Substrates
5 of PKA in the cardiomyocyte include troponin (TNNT2), myosin binding protein c (MYBPC3),
6 phospholamban (PLN), and ryanodine receptor (RYR2) (Marks, 2013). Acute activation of PKA
7 in hyperadrenergic states leads to improved calcium flux and myocardial performance and is
8 necessary for increases in stroke volume to meet cardiac output demands. In heart failure,
9 chronic beta-adrenergic stimulation from high levels of catecholamines results in compensatory
10 downregulation of beta adrenergic signaling to leading diminished phosphorylation of several PKA
11 substrates (Bristow et al., 1982; Piacentino et al., 2003). Long term activation of Pka was shown
12 to be deleterious in mouse models and is thought to underly the maladaptive remodeling of
13 chronic beta-adrenergic activation in heart failure (Antos et al., 2001).

14 STK25 is a stress response kinase in the sterile-20 (Ste20) kinase superfamily and has
15 been shown through a series of *in vivo* models to impact glucose utilization, insulin homeostasis,
16 and lipid metabolism (Amrutkar et al., 2015a; Amrutkar et al., 2015b; Amrutkar et al., 2016a;
17 Amrutkar et al., 2016b; Cansby et al., 2013; Chursa et al., 2017; Nerstedt et al., 2012; Nunez-
18 Duran et al., 2017; Sutt et al., 2018). Overexpression of STK25 leads to steatosis and was shown
19 to aggravate atherosclerosis in a PCSK9 gain of function mouse model (Cansby et al., 2018).
20 Recently, STK25 was shown to interact with the Hippo signaling via phosphorylation of LATS1/2
21 and/or regulation of SAV1-STRIPAK (Bae et al., 2020; Lim et al., 2019). In this study, we use a
22 combination of *in vitro* and *in vivo* cardiomyocytes models to demonstrate that STK25
23 phosphorylates the Type I α regulatory subunit of PKA, PRKAR1A. This leads to increased
24 inhibition of PKA signaling, revealing a new regulatory mechanism that can control PKA activity
25 and attenuate cAMP mediated increases in cardiac contractile function.

26

1 **Methods:**

2 Patient samples

3 Patients with advanced HF were recruited at Columbia University Medical Center and heart tissue
4 at the time of heart transplant was collected from the left ventricle. Control myocardial samples
5 were obtained from the National Disease Research Interchange (<https://ndriresource.org/ats>) and
6 were comprised of de-identified specimens collected from non-failing hearts determined to be
7 unusable for cardiac transplantation due to non-cardiac donor issues but without evidence or
8 knowledge of underlying cardiac disease. The study was approved by the Institutional Review
9 Board of Columbia University (IRB# AAAR0055). All patients provided written informed consent
10 before inclusion into the study.

11

12 Cell culture

13 HEK293T cells (ATCC Cat# CRL-3216, RRID:CVCL_0063) were cultured in high glucose
14 (4.5g/L) DMEM supplemented with 10% FBS, penicillin and streptomycin, and grown in a CO₂
15 incubator maintained at atmospheric oxygen levels and 5% CO₂. Human induced pluripotent
16 stem cells (hiPSC) were obtained through Material Transfer Agreements from Bruce Conklin,
17 Gladstone Institute (WTC cell line). hiPSCs were expanded on growth factor reduced Matrigel-
18 coated plates (Corning) in mTeSR plus medium (Stemcell technologies) containing mTeSR plus
19 supplement (Stemcell technologies), 50U penicillin and 50U streptomycin. The cell culture
20 medium was changed every other day, and cell passaged upon reaching 70% confluence.
21 During the first 24 hrs after passaging, 5 μ M Y-27632 dihydrochloride (Tocris, 1254) was
22 supplemented to culture medium.

23

24 CRISPR-Cas9

25 CRISPR-Cas9 Genome editing was used to generate a homozygous knockout of *STK25* in
26 WTC iPSCs following the manufacturer's protocol (ORIGENE) with gRNA vector (KN203215G).

1 Single-cell clones were expanded and confirmation of homozygous editing was determined by
2 sanger sequencing of gDNA and protein analysis by western blot.

3

4 iPS Cardiomyocyte Differentiation

5 Cardiac differentiation of iPSC's was initiated in confluent monolayers two days after replating at
6 a density of 200,000/cm² (24hrs in mTeSR plus medium with 5µM Y-27632 dihydrochloride,
7 followed by 24hrs in mTeSR plus medium without Y-27632). On day 0 of differentiation, media
8 was changed to cardiac differentiation medium (CDM, consisting of RPMI-1640, Life
9 Technologies), 500µg/ml human recombinant albumin (Sigma), 213µg/ml L-ascorbic acid
10 (Sigma), 50U penicillin and 50U streptomycin) with 3-6 µM CHIR (4423, Tocris). 2 days after
11 initial CHIR addition, media was changed to CDM with 2 µM Wnt-C59 (5148, Tocris). From day
12 4 onwards, media was changed fresh CDM every other day until cells start contracting. Media
13 was then switched to RPMI-B27 (consisting of RPMI-1640, 1x B27 supplement (Life
14 Technologies), 213µg/mL L-ascorbic acid, 50U penicillin and 50U streptomycin). Cardiomyocytes
15 were characterized by flow cytometry using the cardiomyocyte-specific marker TNNT2 (BD
16 Biosciences Cat# 565744, RRID:AB_2739341). Differentiation typically resulted in cell
17 populations containing 80–90% TNNT2-positive cells at day 12.

18

19 PKA activity assay

20 PKA activity assay was performed using whole cell lysate from iPSC-CMs treated with either PBS
21 or 10µM forskolin (Sigma-Aldrich, F6886) for 30min at 37°C prior to assay, or immunoprecipitated
22 type I and II PKA holoenzymes from iPSC-CMs whole cell lysate or whole heart lysates from
23 *Stk25^{+/+}* or *Stk25^{-/-}* mice following the manufacturer's protocol (EIAPKA, Invitrogen). Briefly, PKA
24 standards or diluted samples and reconstituted ATP were added into wells of PKA substrate plate.
25 Phospho-PKA substrate antibody and Goat anti-Rabbit IgG HRP conjugate antibody were added
26 into the wells per manufacturer protocol. After incubation TMB substrate was added into each

1 well, and the plate was incubated for 30 min at room temperature. Stop solution was added, and
2 absorbance at 450nm was analyzed in a 96-plate reader.

3

4 Global Phosphoproteomics analysis

5 Sorted *STK25^{+/+}* and *STK25^{-/-}* iPSC-CMs were lysed/homogenized by bead-beating in 8 M urea,
6 1%SDS and 200 mM EPPS (pH 8.5), protease, and phosphatase inhibitors. Lysates were
7 cleared by centrifugation at 21,000 g for 30 min at 4⁰C, and protein concentration was
8 measured by BCA. Proteins were reduced with 5 mM TCEP, alkylated with 10 mM
9 iodoacetamide (IAA), and quenched with 10 mM DTT. A total of 500 µg of protein was
10 chloroform–methanol precipitated. Protein was reconstituted in 200 mM EPPS (pH 8.5) and
11 digested by Lys-C overnight and trypsin for 6 h, both at a 1:50 protease-to-peptide ratio.
12 Digested peptides were quantified using a Nanodrop at 280 nm, and 200 µg of peptide from
13 each sample were labeled with 800 µg TMT reagent using a 10-plex TMT kit (Navarrete-Perea
14 et al., 2018). TMT labels were checked, 100 ng of each sample was pooled and desalted and
15 analyzed by short SPS-MS3 method, and using normalization factor samples were bulk mixed
16 at 1:1 across all channels and desalted using a 200 mg Sep-Pak solid-phase extraction column
17 and dried using vacuum centrifugation.

18 Desalted isobaric labeled peptides were enriched for phospho-peptides using a mixture
19 of MagReSyn Ti-IMAC and Zr-IMAC resins according ReSyn Bioscience instructions. In brief,
20 1.4 mg of labeled peptide were resuspended in 1 ml of binding buffer (80% Acetonitrile, 1M
21 glycolic acid and 5% TFA) and incubated with equilibrated 150 µl (75 µl of each Ti-IMAC and Zr-
22 IMAC) resins at room temperature for 30 min, and the resin was washed 3 three times to
23 remove the unbound, non-phosphorylated peptides. Phospho-peptides were eluted using 1%
24 ammonium hydroxide. The enriched phospho-peptides were further fractionated in eight
25 fractions using Pierce™ High pH Reversed-Phase Peptide Fractionation Kit and each fraction
26 dried down in a speed-vac.

1 The isobaric labeled dried phospho-peptides were resuspended in 10 μ l of (3%
2 acetonitrile/ 0.1% formic acid), and analyzed on an Orbitrap Fusion mass spectrometer coupled
3 to a Dionex Ultimate 3000 (ThermoFisher Scientific) using the MSA-SPS-MS3 and NL SPS-
4 MS3 method (Jiang et al., 2017). Peptides were separated on an EASY-Spray C18 50cm
5 column (Thermo Scientific). Peptide elution and separation were achieved at a non-linear flow
6 rate of 250 nl/min using a gradient of 5-30% of buffer B (0.1% (v/v) formic acid, 100%
7 acetonitrile) for 110 minutes with a temperature of the column maintained at 50 °C during the
8 entire experiment. For both methods, MS1 data were collected using the Orbitrap (120,000
9 resolution; maximum injection time 50 ms; AGC 4×10^5). Determined charge states between 2
10 and 5 were required for sequencing and a 45 s dynamic exclusion window was used. Data-
11 dependent top10 MS2 scans were performed in the ion trap with collision-induced dissociation
12 (CID) fragmentation (Turbo; NCE 35%; maximum injection time 60ms; AGC 5×10^4). MS3
13 quantification scans were performed using the multi-notch MS3-based TMT method (ten SPS
14 ions; 50,000 resolution; NCE 65% for MSA-SPS-TMT and 38% for NL-SPS-TMT maximum
15 injection time 105 ms; AGC 1×10^5) using the Orbitrap.

16 Raw mass spectrometric data were analyzed using Proteome Discoverer 2.2 to perform
17 database search and TMT reporter ions quantification. TMT tags on lysine residues and
18 peptide N termini (+229.163 Da) and the carbamidomethylation of cysteine residues (+57.021
19 Da) was set as static modifications, while the oxidation of methionine residues (+15.995 Da),
20 deamidation (+0.984) on asparagine and glutamine and phosphorylation (+79.966) on serine,
21 threonine, and tyrosine were set as a variable modification. Data were searched against a
22 UniProt Human database with peptide-spectrum match (PSMs) and protein-level FDR at 1%
23 FDR. The signal-to-noise (S/N) measurements of each protein normalized so that the sum of
24 the signal for all proteins in each channel was equivalent to account for equal protein loading.
25 Phospho-peptides identification and quantification were imported into Perseus (Tyanova et al.,
26 2016) for t-test statistical analysis (FDR<0.05) to identify phospho-peptides demonstrating

1 statistically significant changes in abundance. Pathway analysis were performed using
2 Ingenuity Pathway Analysis (Qiagen).

3

4 Animal studies

5 *Stk25* knockout mice were generated by CRISPR/Cas9 mediated genome engineering in
6 C57BL/6J background (Jackson Laboratory, Bar Harbor, Maine). Exon 3-5 of *Stk25* gene were
7 deleted with two CRISPR guides from Synthego (sgRNA-stk25-7367 and sgRNA-stk25-10150).
8 Both guides were mixed with IDT Cas9V3 protein to form RNP, which was further injected into
9 the pronuclei of fertilized C57BL/6J eggs to generate knockout founders. Genotyping was
10 performed to show the *Stk25* knockout allele. Further breeding generated homozygous *Stk25*^{-/-}
11 mice and protein immunoblotting was performed to confirm an absence of *Stk25*. The protocol for
12 all mouse experiments (AABC1503) was approved by the Columbia University Institutional Animal
13 Care and Use Committee.

14 Cardiac function of 20 week and 52 week old mice was assessed by echocardiography
15 by the Columbia University Mouse Imaging Core Facility (imaged by Visulasonics VEVO 3100
16 High Frequency Ultrasound imaging system and analyzed by Vevo LAB software). For 20 week
17 old mice, cardiac function was recorded at baseline and 3 minutes after administration of the β -
18 adrenergic receptor agonist isoproterenol (0.2ug/g, i.p.). Systolic function parameters including
19 ejection fraction (EF, %), fractional shortening (FS, %), left ventricular end systolic diameter
20 (LVESD, mm) and left ventricular end diastolic diameter (LVEDD, mm) were measured in the two-
21 dimensional parasternal short-axis imaging plane of M-mode tracings close to the papillary
22 muscle level.

23

24 iPS Cardiomyocyte sorting

25 Cardiomyocytes were pretreated with 10 μ M of Y-27632 in B27 culture medium for 6 hrs, then
26 digested with cell dissociation buffer (containing Hank's buffered saline solution, 100 Units/ml

1 collagenase, 10 μ M Y-27632) at room temperature overnight. Cells were collected and
2 centrifuged at 300g for 5 min, and then resuspended in cell sorting buffer (CSB, containing
3 Hank's buffered saline solution, 20mM HEPES, 5% FBS, 10 units/ml Turbo DNase). The cell
4 pellet was resuspended with anti-CD172a/b (SIRP α/β , 423107, Biolegend) and anti-CD90 (Thy-
5 1, 11-0909-42, Invitrogen) antibodies in CSB to stain for 20 min at 4°C in the dark. Cells were
6 washed 3 times with CSB and DAPI staining was added. Cardiomyocytes were sorted from the
7 SIRPA+ and CD90- population and then plated on matrigel coated plates in B27 medium with
8 5 μ M Y-27632. The following day, medium was replaced with fresh B27, and cardiomyocytes
9 generally started to beat in 2-5 days.

10

11 RNA Isolation, Sequencing, and Analysis.

12 RNA was extracted using the RNeasy Mini kit (Qiagen #74004) along with on-column DNase
13 digestion (Qiagen #79254). cDNA libraries were generated using the Clontech Ultra Low v4 kit
14 followed by NextaraXT DNA Library Prep Kit, then sequenced on an Illumina NovaSeq 6000.
15 Paired-end 100-bp sequenced reads were analyzed as follows: RTA (Illumina) software was
16 used for base calling and bcl2fastq2 (version 2.19) for converting BCL to fastq format, coupled
17 with adaptor trimming. A pseudoalignment to a kallisto index created from transcriptomes (build
18 GRCh38) using kallisto (0.44.0). After pseudoalignment the R package DESeq2 (1.28.1) was
19 used to normalize the count matrix and calculate differentially expressed genes. Geneset
20 enrichment analysis was performed using GSEA software (4.10.0) per documentation (Mootha
21 et al., 2003; Subramanian et al., 2005).

22

23 siRNA and vector transfection

24 Cells were transfected using lipofectamine 3000 (Invitrogen) following the manufacturer's
25 protocol with siRNA targeting STK25 (On-TargetPlus siRNA, Horizon Discovery, L-004873-00-
26 0050) or siRNA targeting PRKAR1A (EHU071341, Sigma) for protein knockdown or non-

1 targeting control siRNA (ON-TARGETplus non-targeting pool, Horizon Discovery D-001810-10-
2 50) as scramble control.

3 For heterologous expression studies, cells were transfected using lipofectamine 3000
4 (Invitrogen, L3000015) following the manufacturer's protocol. Vectors used include Flag-WT-
5 STK25 vector (EX-M0142-M46, GeneCopoeia), Flag-K49R/T147A-STK25 vector (Vector
6 Builder), Flag- empty vector (EX-NEG-M46, GeneCopoeia), V5-PRKAR1A (Vector Builder,
7 VB200124-1141aes), V5-S77A/S83A-PRKAR1A (Vector Builder, VB200124-1126jtp), and V5-
8 S77E/S83E-PRKAR1A (Vector Builder, VB200124-1127pst).

9

10 qRT-PCR assays

11 Equivalent amounts (2µg) of purified RNA were used as a template to synthesize cDNA using
12 oligo-d(T) primers and SuperScript™ III First-Strand Synthesis SuperMix (Invitrogen,
13 18080400). *STK25* was quantified by real-time PCR using Fast SYBR Green mixture (Life
14 Technologies, 4385612) and was carried out on Applied Biosystems Step One Plus. Relative
15 levels were calculated using $\Delta\Delta C_T$ method. Data analysis was carried out using the fold change
16 normalized to GAPDH gene expression.

Gene	Forward Primer 5'-3'	Reverse Primer 5'-3'
STK25	GCTCCTACCTAAAGAGCACCA	TGGCAATGTATGTCTCCTCCAG
GAPDH	GGACTCATGACCACAGTCCATG	CAGGGATGATGTTCTGGAGAGC

17

18 Immunoprecipitation and immunoblot analysis

19 300 µg of total protein from whole cell lysate were used in immunoprecipitation experiments.
20 The extract was incubated with anti-Flag affinity gel (Sigma-Aldrich Cat# A2220,
21 RRID:AB_10063035), anti-V5 affinity gel (Sigma-Aldrich Cat# A7345, RRID:AB_10062721),
22 anti-PRKAR1A (Abcam Cat# ab139695, RRID:AB_2893184) or anti-PRKAR2A (ProteinTech
23 Cat# 10142-2-AP) overnight at 4°C. The affinity gel beads were centrifuged at 8000xg for 1min,
24 washed three times in TBS buffer. The affinity gel beads were added with 4x Laemmli SDS

1 sample buffer (NuPAGE), denatured at for 5min at 95°C and analyzed by SDS-PAGE and
2 immunoblotting. For Western blotting antibodies include: HRP conjugated anti-GAPDH (Cell
3 Signaling Technology Cat# 3683, RRID:AB_1642205), anti-STK25 (Abcam Cat# ab157188,
4 RRID:AB_2725788), anti-Flag (Sigma-Aldrich Cat# F3165, RRID:AB_259529), anti-GM130
5 (Cell Signaling Technology Cat# 12480, RRID:AB_2797933), anti- PRKAR1A (Abcam Cat#
6 ab139695, RRID:AB_2893184), anti-pS77 PRKAR1A (Abcam Cat#ab139682,
7 RRID:AB_2904566), anti-pS83 PRKAR1A (Abcam Cat#ab154851, RRID:AB_2904567), anti-
8 PRKAR2A (ProteinTech Cat# 10142-2-AP), anti-phospholamban (Cell Signaling Technology
9 Cat# 14562, RRID:AB_2798511), anti-phospho-phospholamban -pS16/T17 (Cell Signaling
10 Technology Cat# 8496, RRID:AB_10949102), anti-Ryanodine receptor 2 (Abcam
11 Cat#ab196355, RRID:AB_2904568), anti-p- Ryanodine receptor 2-pS2808 (Abcam Cat#
12 ab59225, RRID:AB_946327), anti-Tnl (Cell Signaling Cat# 4002), anti-Tnl-pS23/S24 (Cell
13 Signaling Cat# 4004), anti-V5 (Sigma-Aldrich Cat# V8137, RRID:AB_261889), anti-PKA
14 Catalytic subunit (Abcam Cat# ab26322, RRID:AB_2170049), HRP-conjugated anti-mouse (Cell
15 Signaling Technology Cat# 7076, RRID:AB_330924) and HRP-conjugated anti-rabbit (Cell
16 Signaling Technology Cat# 7074, RRID:AB_2099233) were used for detection.

17

18 In vitro kinase assay

19 Recombinant protein STK25 (0.5µM, TP303215, OriGene) and PRKAR1A (1µM, TP303828
20 Origene) were mixed with *in vitro* kinase buffer (25mM Tris-HCl, 10mM beta-glycerophosphate,
21 10mM MgCl₂, 20mM NaF, 2mM DTT, 1mM sodium orthovanadate, 1x Protease Inhibitor cocktail
22 (Roche)) containing ATP (500uM) and incubated at 37°C for 30 min. In vitro kinase assay was
23 terminated by adding Laemmli SDS sample buffer. Phosphorylation levels of PRKAR1A at S77
24 and S83 were analyzed by SDS-PAGE and immunoblotting.

25

26 Real Time Glo cell viability assay

1 Cells were seeded into 96-well plates at a density of 3000 cells per well 24h before
2 measurement. RealTime-Glo (Promega; G9712) reagent was added to each well per
3 manufacturer protocol and measurement of luminescence was performed at selected time
4 points on a BioTek Synergy JHTX with Gen5 data analysis software.

5

6 **Statistical Analysis:**

7 Statistical analyses were performed using Prism 8 (Graphpad Software). Results are presented
8 as mean \pm standard deviation. For comparisons between two groups, a two tailed unpaired t-
9 test was used unless otherwise specific. Welch's correction was utilized for two groups of
10 unequal sizes. For multiple group comparisons, either one way or two-way (depending on the
11 number of variables) ANOVA followed by multiple comparison post-hoc testing was performed
12 as indicated using Prism 8. Notation in the text is as follows * $p < 0.05$, ** $p < 0.01$, *** $p < 0.001$ and
13 **** $p < 0.0001$

14

15

16

17 **Results:**

18 **STK25 inhibits PKA signaling.**

19 As part of an kinome knockout discovery project, CRISPR-Cas9 was used to generate a
20 homozygous knockout of *STK25* in the wild type iPSC line WTC11 (Bruce Conklin, Gladstone
21 Institute) (Hayashi et al., 2016), and cardiomyocytes were differentiated and characterized using
22 an established protocol (Burrige et al., 2014). *STK25* expression in iPSC derived
23 cardiomyocytes was found to be similar to *Stk25* expression to primary cardiomyocytes from adult
24 mice (**Figure S1A and S1B**). To identify potential substrates of STK25 in cardiomyocytes, mass
25 spectrometry based phosphoproteomics was performed with *STK25*^{+/+} and *STK25*^{-/-}
26 cardiomyocytes (**Figure 1A**). Signaling pathways impacted by *STK25* were identified using

1 Ingenuity Pathway Analysis (Qiagen). A decrease in Hippo signaling was observed in response
2 to loss of STK25 confirming a prior study demonstrating STK25 activates the Hippo pathway
3 (**Figure 1B**) (Lim et al., 2019). The most significant signaling change in response to loss of *STK25*
4 was an upregulation of the PKA pathway. Several downstream substrates of PKA displayed
5 increased phosphorylation including MYBPC3, TNNT2, RYR2, CACNA1C and GSK3 α (**Table 1**).
6 *STK25*^{-/-} cardiomyocytes exhibited increased PKA kinase activity when stimulated with the
7 adenylate cyclase agonist forskolin (**Figure 1C**). In heterologous overexpression studies in
8 HEK293T cells, STK25 decreased forskolin induced PKA activity. This inhibition was dependent
9 on the kinase domain of STK25 as overexpression of the kinase-dead mutant *STK25*^{K49R/T174A}
10 (Preisinger et al., 2004) did not inhibit PKA activity in response to forskolin (**Figure 1D**).

11

12 **STK25 phosphorylates PRKAR1A**

13 Two of the most downregulated phosphorylation sites in *STK25*^{-/-} iPSC-CM were S77 and
14 S83 of PRKAR1A raising the possibility that these sites were directly phosphorylated by STK25
15 (**Table 1**). PRKAR1A is the R1 α member of the regulatory subunit isoforms of the PKA
16 holoenzyme which binds to and inhibits the catalytic subunit of PKA (PRKACA) and has been
17 shown to disengage in response to cAMP, leading to PKA activation (Bossis and Stratakis, 2004).
18 We first confirmed the phosphoproteomic data by demonstrating decreased phosphorylation of
19 S77 and S83 in *STK25*^{-/-} cardiomyocytes by immunoblot protein analysis (**Figure 2A and S2A**).
20 In order to determine if this observation was dependent on the kinase activity of STK25,
21 *STK25*^{K49R/T174A} was expressed in *STK25*^{-/-} iPSC-CMs and led to significantly decreased
22 phosphorylation of S77 and S83 compared to overexpression of wild type STK25 (**Figure 2B and**
23 **S2B**). Stimulation of PKA with forskolin led to diminished phosphorylation at both S77 and S83
24 in *STK25*^{+/+} iPSC-CM but did not have significant effect on *STK25*^{-/-} iPSC-CMs (**Figure 2C and**
25 **S2C**).

1 Co-immunoprecipitations experiments demonstrated STK25 and PRKAR1A binding using
2 epitope tagged protein in HEK293T cells (**Figure 2D**). Though forskolin inhibited binding between
3 PRKAR1A and the catalytic subunit, PRKACA, it did not alter the association between STK25 and
4 PRKAR1A (**Figure 2E**). Mutation of the kinase domain of STK25 also did not affect binding to
5 PRKAR1A by immunoprecipitation (**Figure S2D**). Using purified protein in an *in vitro* kinase
6 assay, STK25 was able to phosphorylate PRKAR1A at S77 and S83(**Figure 2F**).

7

8 **Phosphorylation of S77/S83 inhibits PKA activity**

9 Phosphorylation at S77 and S83 on PRKAR1A have been described as part of large scale global
10 phosphoproteomic experiments (Bian et al., 2014; Daub et al., 2008; Olsen et al., 2006;
11 Oppermann et al., 2009) but their influence on PKA activity has not been characterized. In order
12 to investigate the effect of pS77 and pS83 on the ability of PRKAR1A to inhibit PKA activity,
13 phosphomimetic (S77E/S83E) and non-phosphomimetic (S77A/S83A) mutations were generated
14 in PRKAR1A expression vectors. In HEK293T co-immunoprecipitation experiments, all three
15 isoforms bind PRKACA similarly (**Figure S3A and S3B**). However, upon stimulation with forskolin
16 the S77E/S83E mutant exhibited elevated binding to the catalytic subunit compared to the
17 S77A/S83A and WT PRKAR1A, indicating that positive charges at this residue may interfere with
18 release of PKA in response to cAMP (**Figure 3A and S3C**). We then further tested this hypothesis
19 by assessing PKA kinase activity *in vitro* in response to overexpression of these constructs in
20 HEK293T cells. Though both WT and S77A/S83A PRKAR1A exhibited attenuated increases in
21 induced PKA activity, expression of the S77E/S83E mutant exhibited no increase in PKA activity
22 in response to forskolin (**Figure 3B**). Similarly, S77E/S83E PRKAR1A was able to inhibit
23 metabolic activity of HEK293T in response to forskolin (**Figure 3C**) and in normal growth
24 conditions (**Figure S3D**) to a significantly greater degree than either PRKAR1A or STK25
25 overexpression alone. In order to confirm that PRKAR1A is downstream of STK25, STK25 was
26 overexpressed simultaneously with knock-down of PRKAR1A resulting in rescue of STK25

1 inhibition of PKA activity (**Figure 3D and Figure S3E**). Together these data demonstrate a new
2 regulatory event where STK25 phosphorylation increases the ability of PRKAR1A to bind the
3 catalytic subunit and inhibit PKA activity in response to cAMP (**Figure 3E**).

4 Phosphorylation of PRKAR2A was also detected in our phosphoproteomic analysis
5 however phosphorylation levels increased with the loss of STK25 (**Table 1**). Despite this, given
6 its role in PKA regulation in cardiomyocytes, we evaluated PKA holoenzyme activity from
7 PRKAR1A and PRKAR2A immunoprecipitates. Loss of STK25 increased PKA activity from
8 PRKAR1A complexes but not PRKAR2A complexes (**Figure S4A and S4B**). Furthermore,
9 immunoprecipitation experiments did not demonstrate binding of PRKAR2A and STK25 (**Figure**
10 **2D**). Together these data do not support PRKAR2A as a downstream effector of STK25.

11

12 ***Stk25* loss increases PKA activity *in vivo***

13 In order to validate the STK25-PKA relationship *in vivo*, we generated an *Stk25*^{-/-} mouse and
14 investigated the impact of *Stk25* loss on the Pka pathway *in vivo*. Protein analysis demonstrated
15 that loss of *Stk25* was accompanied by an increase in Prkar1a levels and a significant decrease
16 in the ratio of pS77 and pS83 to total Prkar1a (**Figure 4A and S5A**). Whole heart lysates of
17 *Stk25*^{-/-} mice displayed increased levels of Pka kinase activity compared to wildtype littermates
18 (**Figure 4B**). Hearts histologically were similar without any fibrosis (**Figure S5B**) and heart weight
19 to body weight ratio were not different between genotypes (**Figure S5C**).

20 Since Pka mediates beta adrenergic stimulation of cardiomyocyte contraction function *in*
21 *vivo*, we assessed the impact of *Stk25* loss on cardiac function in response to the β 1 agonist
22 isoproterenol using echocardiography. At baseline, there were no significant differences in either
23 contractile function or chamber dimensions between genotypes; however *Stk25*^{-/-} mice displayed
24 statistically greater individual increases in ejection fraction (EF) and fractional shortening (FS)
25 and trends towards decreased chamber size in response to isoproterenol (**Figure 4C, 4D and**
26 **S5D**). Phosphorylation levels of downstream Pka effectors were also evaluated in response to

1 isoproterenol and loss of *Stk25* was associated with significant increases in isoproterenol induced
2 phosphorylation of Pln, Tnl, and Ryr2 while CamKII remained unchanged (**Figure S6A and S6B**).

3 Because prolonged Pka activation has been associated with heart failure (Antos et al.,
4 2001; Kushnir et al., 2010), a survival cohort of mice at 52 weeks were evaluated by
5 echocardiography and no significant differences in either heart function or left ventricular size
6 were found (**Figure S7**). We then investigated human heart failure samples and found that *STK25*
7 expression was broadly *increased* in myocardial samples from patients with end stage heart
8 failure when compared to normal heart samples (**Figure 4E and Table S1**). Using available
9 protein samples from this heart failure cohort, we analyzed the phosphorylation status of
10 PRKAR1A and observed a concordant increase in *STK25*, PRKAR1A and phosphorylated
11 PRKAR1A. This raises the possibility that upregulation of *STK25* and PRKAR1A has a role in
12 heart failure and may be involved in the compensatory downregulation of beta adrenergic
13 signaling.

14

15 **Discussion**

16 Kinases are integral components of signal transduction pathways, playing key roles in
17 most cellular processes that are initiated by external cues. Therapeutic modulation of kinases
18 has demonstrated success in many branches of medicine, highlighted especially by those that
19 leverage inhibition of kinase cascades implicated in oncogenic processes. Within cardiovascular
20 biology, kinases regulate ion handling, contractility, and metabolism, and their dysregulation is
21 involved in many cardiovascular diseases (Clerk et al., 2007; Heineke and Molkentin, 2006;
22 Vlahos et al., 2003). Several kinases including PKA, Ca²⁺ calmodulin dependent kinase, protein
23 kinase C and PIP3 kinase have all been implicated in both physiologic and pathologic signaling
24 (Dhalla and Muller, 2010). Despite this progress, kinase directed therapy has not been developed
25 successfully for cardiovascular diseases, and identifying new regulators of kinase pathways is an
26 area of unrealized therapeutic potential.

1 Here we present evidence that STK25 is an inhibitor of the PKA pathway, whose
2 phosphorylation of a regulatory subunit drives inhibition of the catalytic subunit's kinase activity.
3 Though phosphorylation of the Type II regulatory subunits has been described in detail, little is
4 known about phosphorylation of Type I regulatory subunits. Phosphorylation at S103 *in vitro* has
5 been shown to be mediated by protein kinase G and interferes potentially with binding to PRKACA
6 (Haushalter et al., 2018). Phosphorylation at S83 has been shown to modulate PRKAR1A's
7 association with the replication factor c complex *in vitro*, the consequence of which is unknown
8 (Gupte et al., 2006). In the model we propose, phosphorylation at S77 and S83 increases affinity
9 of PRKAR1A for the catalytic subunit and inhibits cAMP mediated PKA activity. This stands in
10 contrast to the regulation of Type II subunits whose phosphorylation promotes release of the
11 catalytic subunit and thus enhances PKA activity.

12 Though chronic PKA activation has been associated with progression of heart failure in
13 animal models (Marks, 2013), knockout of *Stk25* resulted in an increase in PKA activity without
14 evidence of heart failure. This discrepancy merits discussion. First it should be noted that heart
15 failure mouse models overexpressing the catalytic PKA subunit generate up to 8-fold increases
16 in PKA activity while in our model, mice experience approximately a 1.6-fold increase in PKA
17 activity. This is in range of prior work demonstrating no heart failure phenotype with *Prkar1a*
18 heterozygosity despite an increase in PKA activity by approximately 1.4-fold (Liu et al., 2020).
19 Furthermore, data from human heart failure samples demonstrate *decreased* phosphorylation of
20 PKA targets (Najafi et al., 2016) as chronic hyperstimulation of the beta-adrenergic receptor leads
21 to desensitization and what is thought to be decreased PKA substrate activation (Ungerer et al.,
22 1993). We observe *increased* levels of STK25 and phosphorylated PRKAR1A in heart failure
23 samples. This would translate into suppression of PKA stimulation yet it remains to be seen
24 whether these changes are protective (e.g. as part of a downregulation response to
25 hyperadrenergic state of heart failure) versus maladaptive (e.g. higher levels of STK25 lead to
26 worsening cardiac performance) or both. While, differences in either heart function or mortality

1 are not observed with loss of *Stk25*, further longitudinal studies with overlaid chronic heart
2 failure models are needed to determine if sustained STK25 loss is a potential therapeutic to
3 improve cardiac function safely.

4

5 *Limitations*

6 There are several important limitations to this study. How exactly phosphorylation of
7 PRKAR1A alters its ability to inhibit the catalytic subunits remains unclear. We observe increased
8 binding of S77E/S83E to the catalytic subunits in forskolin stimulated cells which implies there is
9 either increased affinity between PRKAR1A and the catalytic subunit versus decreased affinity
10 for cAMP by phosphorylated PRKAR1A. Another possibility is a change in PRKAR1A's affinity
11 for an AKAP. Though Type I regulatory subunits generally have weak affinities for AKAP proteins
12 and display a diffuse cytoplasmic localization, the impact that phosphorylation on the assembly
13 of a larger macromolecular regulatory complex remains to be investigated. This is particularly
14 relevant since forskolin did not inhibit PRKAR1A and STK25 binding, yet PRKAR1A
15 phosphorylation was diminished. This would imply that there is either inhibition of STK25 kinase
16 activity by cAMP or a phosphatase that acts on PRKAR1A that is stimulated by cAMP. Given that
17 we observe residual phosphorylation of S77 and S83 in both iPSC-CM and mouse knockout
18 studies, it is likely that there are other kinases that phosphorylate these sites and regulate PKA
19 activity. Further studies are needed to elucidate kinases and phosphatases modulate the
20 phosphorylation status of PRKAR1A what their physiological role is in PKA activity in the heart.

21

22 In summary, loss of *STK25* leads to increased PKA activity *in vitro* and *in vivo*. We identify
23 PRKAR1A as a new substrate for STK25 and demonstrate that phosphorylation of PRKAR1A at
24 S77 and S83 inhibits PKA signaling. Loss of *Stk25* leads to increased physiologic response to
25 beta adrenergic stimulation of cardiac function without evidence of heart failure. Both STK25 and

1 the phosphorylation of PRKAR1A are upregulated in heart failure and potentially represent a new
2 pathway for downregulation of beta adrenergic signaling in the heart.

3
4

5 **Acknowledgements**

6
7 We would like to thank the Qing Li for his surgical expertise, Erin Bush at the Columbia Genome
8 Center for RNA-seq help, Christopher Damoci at the Columbia Mouse Imaging Core Facility and
9 the labs of Veli Topkara, Elain Wan and Emily Tsai for reagents, technical expertise and tissue
10 samples. B.F is supported by a grant from the NHLBI (K08HL140201), the Gerstner Foundation
11 and the Schwartz Foundation. G.V.N is supported by grants from the NIH (UH3EB025765,
12 P41EB027062, and R01HL076485) and NSF (NSF16478). B.W. T.N and B.L are supported by
13 the MSTP Training Program (T32GM007367). B.L. is also supported by the NIH (F30HL145921).
14 R.K.S is supported by 2P30 CA013696-45 Cancer Center Support Grant. M.K. is supported by
15 a Glorney Raisbeck Fellowship Award in Cardiovascular Disease.

16

17 **Competing Interests: None**

18

19 **Data Availability.**

20 RNA-seq data has been deposited in the Gene Expression Omnibus, NCBI: GSE195514

21 Proteomics data has been deposited in the PRIDE ProteomeXchange: PXD031367

22 Original Data can be found at:

23 [https://data.mendeley.com/datasets/t2z9bkm78h/draft?a=a7e3489f-7112-4504-94a4-](https://data.mendeley.com/datasets/t2z9bkm78h/draft?a=a7e3489f-7112-4504-94a4-33f48aa43867)

24 [33f48aa43867](https://data.mendeley.com/datasets/t2z9bkm78h/draft?a=a7e3489f-7112-4504-94a4-33f48aa43867)

25

26 **Material Availability**

27 All unique reagents generated in this study are available from the lead contact with a completed
28 materials transfer agreement.

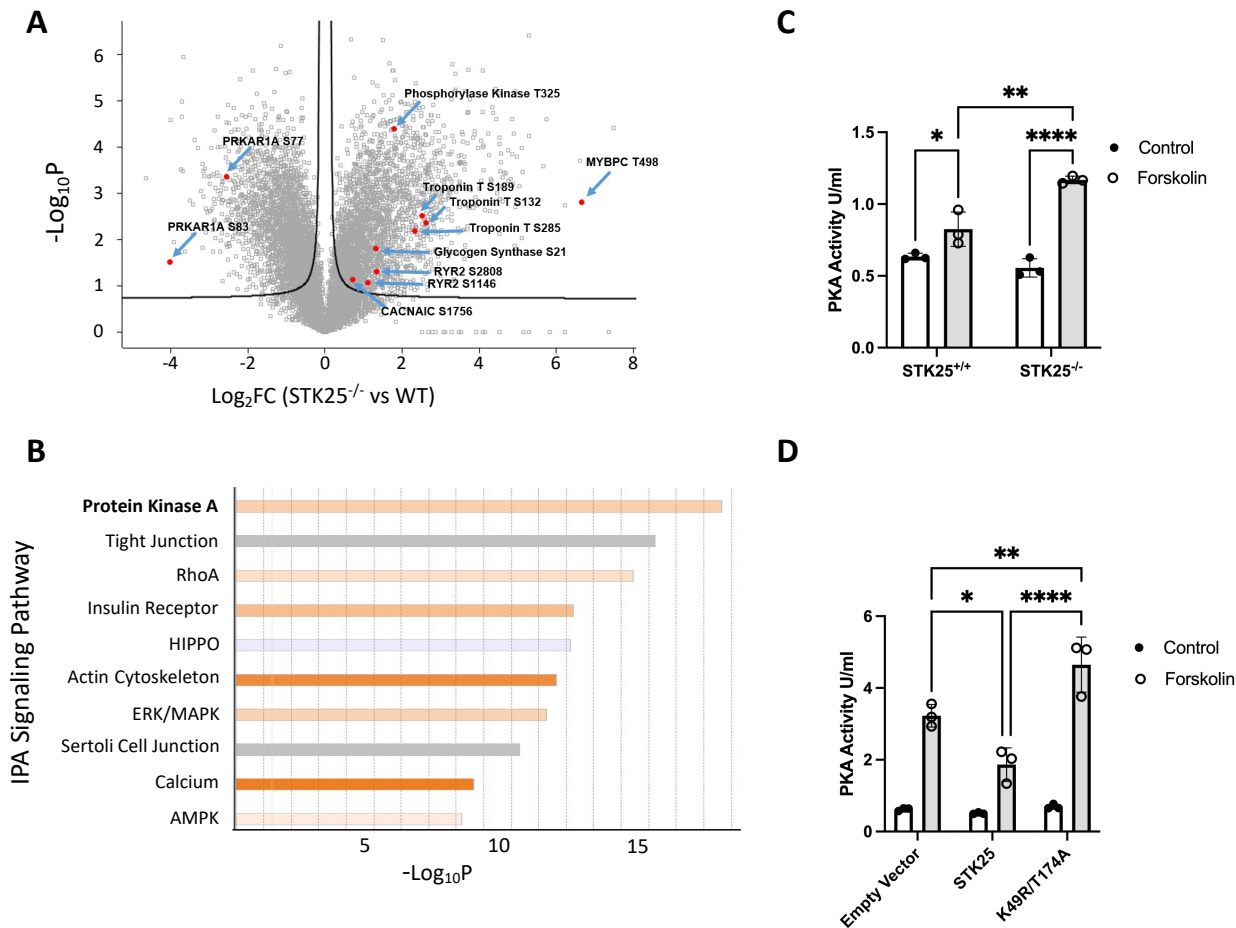


Figure 1. *STK25* inhibits PKA activity. A) Differential phosphoproteomic spectra of *STK25*^{+/+} and *STK25*^{-/-} cardiomyocytes. Members of the PKA signaling pathway are highlighted. B) Ingenuity phosphoprotein pathway analysis. Orange indicates pathways upregulated in *STK25*^{-/-} cardiomyocytes while blue indicates upregulation in *STK25*^{+/+}. C) PKA activity in response to 10 μM forskolin treatment for 30 minutes in *STK25*^{+/+} and *STK25*^{-/-} cardiomyocytes. $n=3$ for each condition. D) PKA activity in response to 10 μM forskolin treatment for 30 minutes in HEK293T cells overexpressing either empty vector, wild type *STK25* or kinase-dead K49R/T174A. $n=3$ for each condition. Bar graph data is represented as mean \pm SD, * $p < 0.05$ ** $p < 0.01$, **** $p < 0.0001$ using ANOVA and Tukey's adjustment for multiple comparisons.

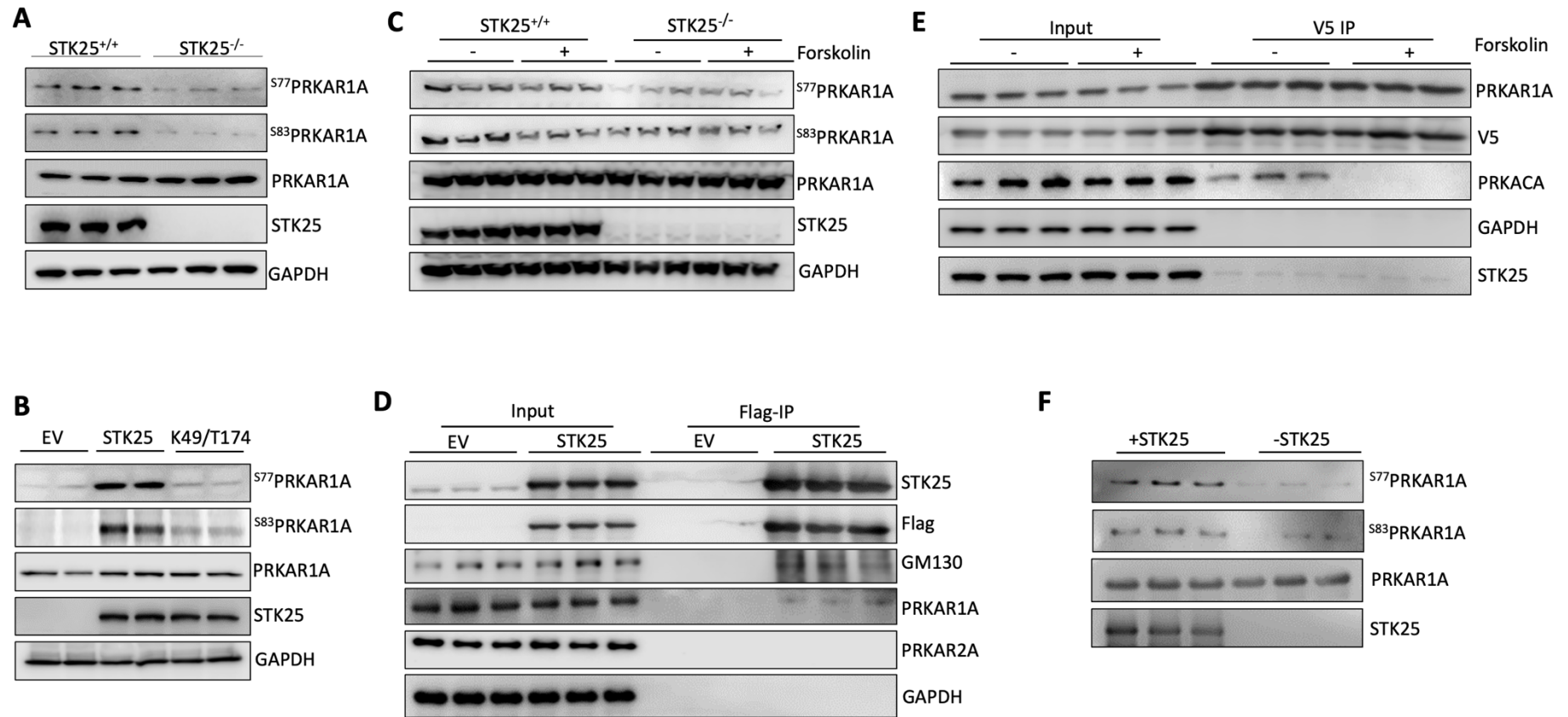


Figure 2. *STK25 binds to and phosphorylates PRKAR1A.* A) Immunoblot of PRKAR1A phospho-S77 and S83 in *STK25*^{+/+} and *STK25*^{-/-} cardiomyocyte protein lysates. B) Immunoblots of phospho-S77 and S83 of PRKAR1A in *STK25*^{-/-} cardiomyocytes transfected with empty vector (EV), wild type STK25 and kinase dead K49R/T174A STK25. C) Forskolin (10 μM, 30 minutes) stimulated *STK25*^{+/+} and *STK25*^{-/-} cardiomyocytes immunoblotted for phosphorylation of PRKAR1A. D) Immunoprecipitation of Flag-STK25 expressed in HEK293T cells and immunoblotted for PRKAR1A, PRKAR2A and GM130 (positive control binding partner). E) Co-immunoprecipitation of PRKAR1A-V5 with STK25 and PRKACA in HEK293T cells treated with forskolin (10 μM, 30 minutes). F) *In vitro* kinase assay of purified STK25 and PRKAR1A, immunoblotted for phosphorylation of S77 and S83 of PRKAR1A.

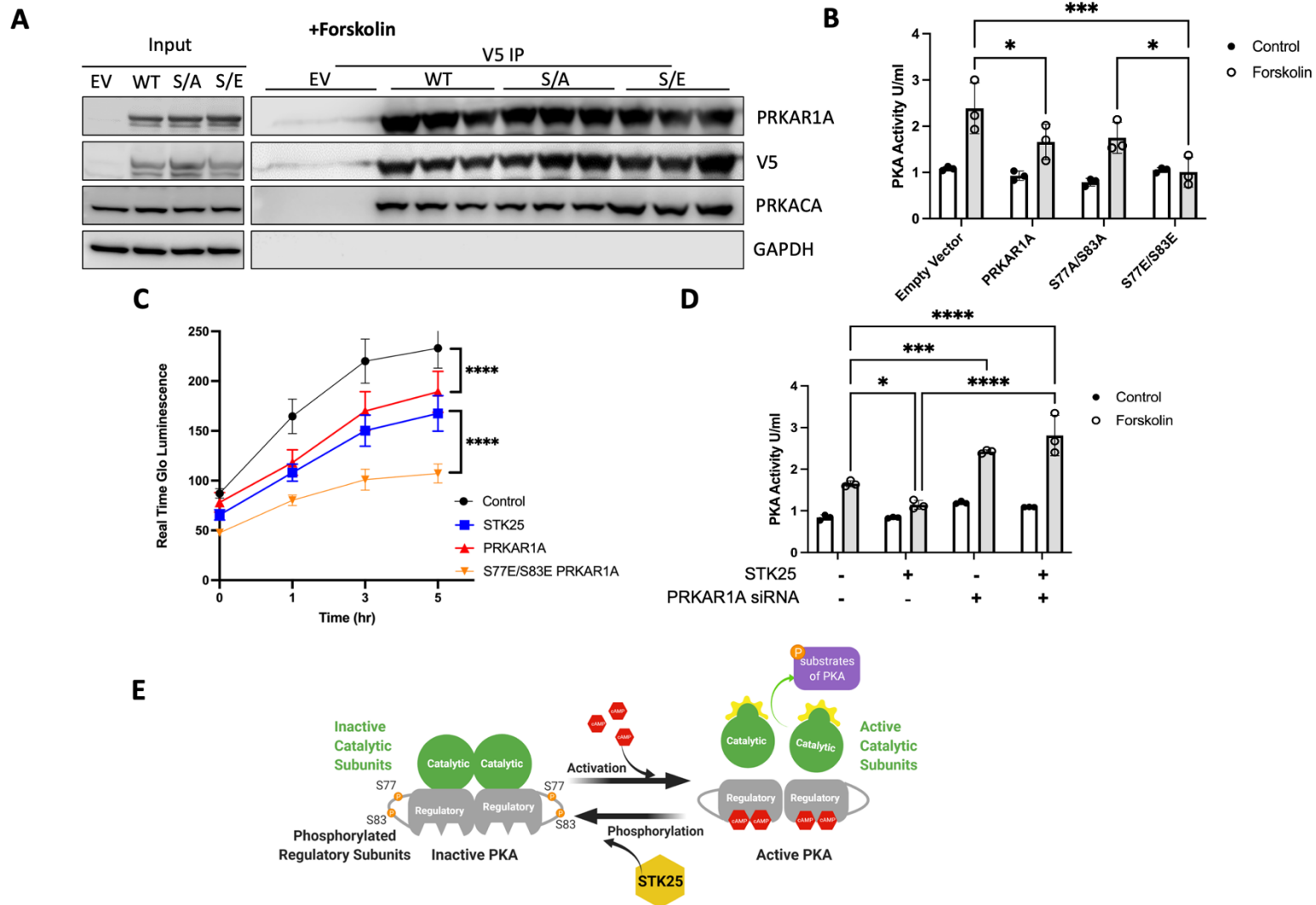


Figure 3. Phosphorylation of PRKAR1A inhibits PKA activity. A) Co-immunoprecipitations of V5 tagged PRKAR1A, S77A/S83A PRKAR1A or S77E/S83E PRKAR1A and immunoblotting for PRKAR1A in HEK293T cells stimulated with forskolin (10 μ M, 30 minutes). B) PKA activity in HEK293T cells stimulated with forskolin (10 μ M, 30 minutes) and transfected with empty vector, wild type PRKAR1A, S77A/S83A PRKAR1A mutant or S77E/S83E PRKAR1A mutant as indicated. C) HEK293T cells transfected with the indicated vectors and assessed for growth by Real Time Glo for 5 hours after stimulation with forskolin (10 μ M). D) PKA activity in HEK293T cells stimulated with forskolin (10 μ M, 30 minutes) and either overexpressing STK25 and/or the siRNA of PRKAR1A. E) Model of STK25 downregulation of the PKA pathway through phosphorylation of PRKAR1A. For all graphs in this figure, n=3 for each condition, data presented as mean +/- SD *p<0.05, ***p<0.001, and ****p<0.0001 by ANOVA with Tukey's adjustment for multiple comparisons.

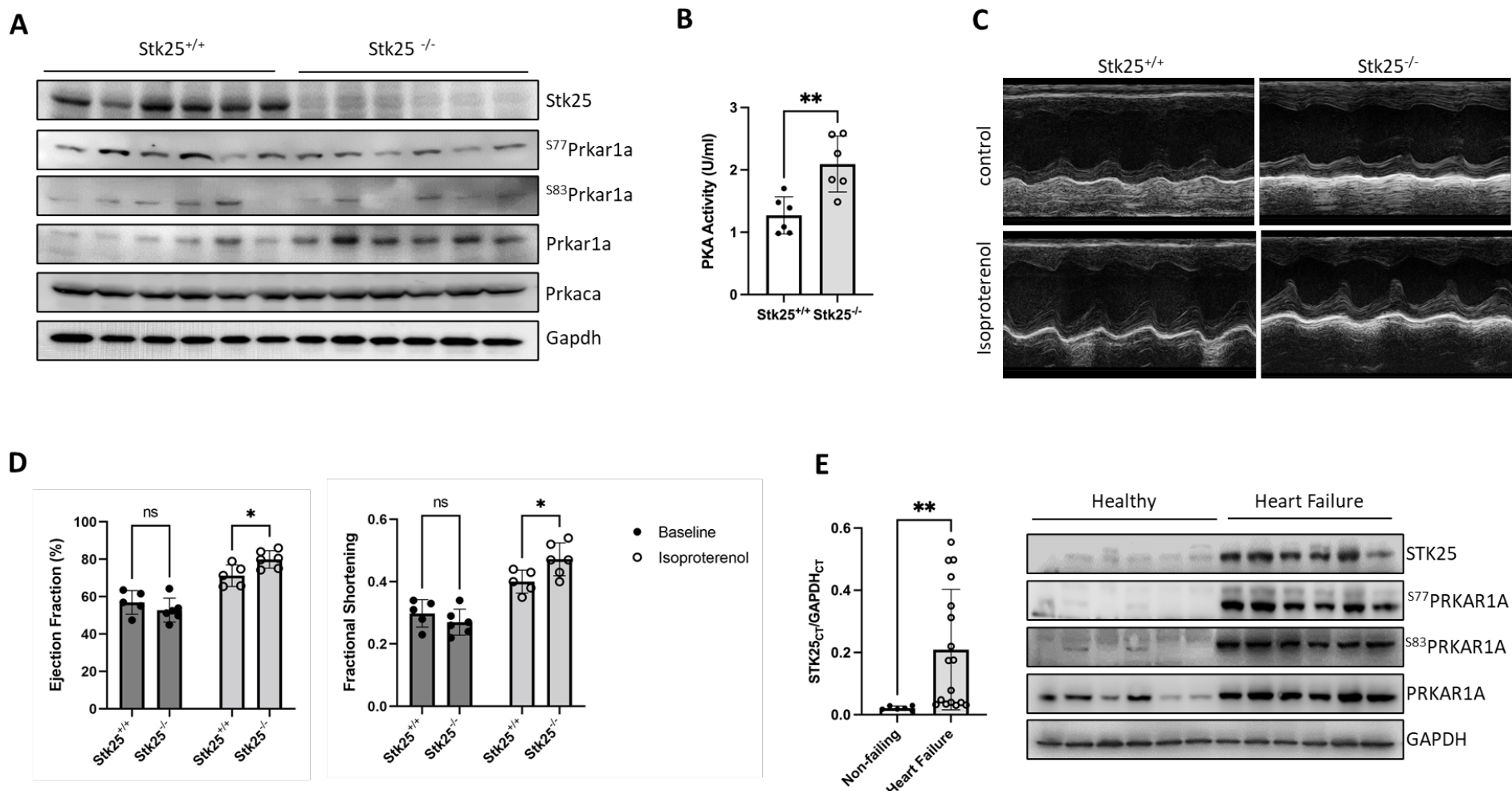


Figure 4. *Stk25* loss increases response to adrenergic stimulation *in vivo*. A) Immunoblot of Stk25, Prkaca, Gapdh, phospho-S77, phospho-S83 and total Prkar1a in *Stk25*^{+/+} and *Stk25*^{-/-} whole heart lysates. B) *Stk25*^{+/+} and *Stk25*^{-/-} mouse heart lysates were assessed for PKA activity *in vitro*, n=6 for each condition. C) Representative m-mode images of *Stk25*^{+/+} and *Stk25*^{-/-} mouse hearts stimulated with either control or isoproterenol. D) Echocardiographic measurements of ejection fraction (EF) and fractional shortening (FS) at unstimulated baseline and in response to isoproterenol, n=5 for *Stk25*^{+/+} and n=6 for *Stk25*^{-/-}. E) RT-PCR (left) from left ventricular myocardium of normal hearts (n=6) or heart failure (n=17) expressed as a ratio of the threshold cycle curve (Ct) of *STK25* to *GAPDH*. Immunoblot (right) of *STK25* and *PRKAR1A* expression and phosphorylation in protein lysates from left ventricular myocardium of normal hearts or failing hearts. Bar graphs presented as mean +/- SD, *p<0.05, **p<0.01 by student t-test in 4B, repeated measures 2 way ANOVA with Sidak's correction for multiple comparisons in 4D and Welch's t-test in 4E.

Function		Protein Descriptions		Fold Change	Phosphorylation Sites	Protein Accessions
PKA	Regulatory subunits	PRKAR1A	cAMP-dependent protein kinase type I-alpha regulatory subunit	0.17	S77, S83	P10644
		PRKAR2A	cAMP-dependent protein kinase type II-alpha regulatory subunit	3.03	S78	P13861
	Catalytic Subunit	PRKACA	cAMP-dependent protein kinase catalytic subunit alpha	0.79	S339	P17612
PKA targets	Contractility Ca ²⁺ handling	MYBPC	Myosin-binding protein C, cardiac-type	100.03	T498	Q14896
		Troponin	Troponin T, cardiac muscle	6.18	S132	P45379
				5.75	S285	
				5.02	S189	
	RYR2	Isoform 2 of Ryanodine receptor 2	2.51	S2808	Q92736	
	2.14	S4368				
	CACNA1C	Isoform 2 of Voltage-dependent L-type calcium channel subunit alpha-1C	1.65	S1756	Q13936	
Energy Metabolism	Phosphorylase Kinase	Phosphorylase b kinase gamma catalytic chain	3.48	T325	P15735	
	Glycogen Synthase	Glycogen synthase kinase-3 alpha	2.50	S21	P49840	
Gene Expression	CREB	Cyclic AMP-responsive element-binding protein 1	0.79	S271	P16220	

Table 1: PKA pathway phosphoproteomic changes in STK25^{-/-} compared to wild type. Fold change represents a ratio of STK25^{-/-}/STK25^{+/+}. Phosphorylation sites, description and accession numbers for each uniprot ID are listed. All changes met a significance threshold of an FDR corrected q value <0.05.

References

- Amrutkar, M., Cansby, E., Chursa, U., Nunez-Duran, E., Chanclon, B., Stahlman, M., Friden, V., Manneras-Holm, L., Wickman, A., Smith, U., *et al.* (2015a). Genetic Disruption of Protein Kinase STK25 Ameliorates Metabolic Defects in a Diet-Induced Type 2 Diabetes Model. *Diabetes* *64*, 2791-2804.
- Amrutkar, M., Cansby, E., Nunez-Duran, E., Pirazzi, C., Stahlman, M., Stenfeldt, E., Smith, U., Boren, J., and Mahlapuu, M. (2015b). Protein kinase STK25 regulates hepatic lipid partitioning and progression of liver steatosis and NASH. *FASEB J* *29*, 1564-1576.
- Amrutkar, M., Chursa, U., Kern, M., Nunez-Duran, E., Stahlman, M., Sutt, S., Boren, J., Johansson, B.R., Marschall, H.U., Bluher, M., *et al.* (2016a). STK25 is a critical determinant in nonalcoholic steatohepatitis. *FASEB J* *30*, 3628-3643.
- Amrutkar, M., Kern, M., Nunez-Duran, E., Stahlman, M., Cansby, E., Chursa, U., Stenfeldt, E., Boren, J., Bluher, M., and Mahlapuu, M. (2016b). Protein kinase STK25 controls lipid partitioning in hepatocytes and correlates with liver fat content in humans. *Diabetologia* *59*, 341-353.
- Antos, C.L., Frey, N., Marx, S.O., Reiken, S., Gaburjakova, M., Richardson, J.A., Marks, A.R., and Olson, E.N. (2001). Dilated cardiomyopathy and sudden death resulting from constitutive activation of protein kinase a. *Circ Res* *89*, 997-1004.
- Bae, S.J., Ni, L., and Luo, X. (2020). STK25 suppresses Hippo signaling by regulating SAV1-STRIPAK antagonism. *Elife* *9*.
- Barradeau, S., Imaizumi-Scherrer, T., Weiss, M.C., and Faust, D.M. (2002). Intracellular targeting of the type-I alpha regulatory subunit of cAMP-dependent protein kinase. *Trends Cardiovasc Med* *12*, 235-241.
- Bian, Y., Song, C., Cheng, K., Dong, M., Wang, F., Huang, J., Sun, D., Wang, L., Ye, M., and Zou, H. (2014). An enzyme assisted RP-RPLC approach for in-depth analysis of human liver phosphoproteome. *J Proteomics* *96*, 253-262.
- Bossis, I., and Stratakis, C.A. (2004). Minireview: PRKAR1A: normal and abnormal functions. *Endocrinology* *145*, 5452-5458.
- Bristow, M.R., Ginsburg, R., Minobe, W., Cubicciotti, R.S., Sageman, W.S., Lurie, K., Billingham, M.E., Harrison, D.C., and Stinson, E.B. (1982). Decreased catecholamine sensitivity and beta-adrenergic-receptor density in failing human hearts. *N Engl J Med* *307*, 205-211.
- BurrIDGE, P.W., Matsa, E., Shukla, P., Lin, Z.C., Churko, J.M., Ebert, A.D., Lan, F., Diecke, S., Huber, B., Mordwinkin, N.M., *et al.* (2014). Chemically defined generation of human cardiomyocytes. *Nat Methods* *11*, 855-860.
- Cansby, E., Amrutkar, M., Manneras Holm, L., Nerstedt, A., Reyahi, A., Stenfeldt, E., Boren, J., Carlsson, P., Smith, U., Zierath, J.R., *et al.* (2013). Increased expression of STK25 leads to impaired glucose utilization and insulin sensitivity in mice challenged with a high-fat diet. *FASEB J* *27*, 3660-3671.
- Cansby, E., Magnusson, E., Nunez-Duran, E., Amrutkar, M., Pedrelli, M., Parini, P., Hoffmann, J., Stahlman, M., Howell, B.W., Marschall, H.U., *et al.* (2018). STK25 Regulates Cardiovascular Disease Progression in a Mouse Model of Hypercholesterolemia. *Arterioscler Thromb Vasc Biol* *38*, 1723-1737.
- Chursa, U., Nunez-Duran, E., Cansby, E., Amrutkar, M., Sutt, S., Stahlman, M., Olsson, B.M., Boren, J., Johansson, M.E., Backhed, F., *et al.* (2017). Overexpression of protein kinase STK25 in mice exacerbates ectopic lipid accumulation, mitochondrial dysfunction and insulin resistance in skeletal muscle. *Diabetologia* *60*, 553-567.

- Clerk, A., Cullingford, T.E., Fuller, S.J., Giraldo, A., Markou, T., Pikkarainen, S., and Sugden, P.H. (2007). Signaling pathways mediating cardiac myocyte gene expression in physiological and stress responses. *J Cell Physiol* 212, 311-322.
- Colledge, M., and Scott, J.D. (1999). AKAPs: from structure to function. *Trends Cell Biol* 9, 216-221.
- Daub, H., Olsen, J.V., Bairlein, M., Gnad, F., Oppermann, F.S., Korner, R., Greff, Z., Keri, G., Stemmann, O., and Mann, M. (2008). Kinase-selective enrichment enables quantitative phosphoproteomics of the kinome across the cell cycle. *Mol Cell* 31, 438-448.
- Dhalla, N.S., and Muller, A.L. (2010). Protein Kinases as Drug Development Targets for Heart Disease Therapy. *Pharmaceuticals (Basel)* 3, 2111-2145.
- Gancedo, J.M. (2013). Biological roles of cAMP: variations on a theme in the different kingdoms of life. *Biol Rev Camb Philos Soc* 88, 645-668.
- Gupte, R.S., Traganos, F., Darzynkiewicz, Z., and Lee, M.Y. (2006). Phosphorylation of RIalpha by cyclin-dependent kinase CDK 2/cyclin E modulates the dissociation of the RIalpha-RFC40 complex. *Cell Cycle* 5, 653-660.
- Haushalter, K.J., Casteel, D.E., Raffener, A., Stefan, E., Patel, H.H., and Taylor, S.S. (2018). Phosphorylation of protein kinase A (PKA) regulatory subunit RIalpha by protein kinase G (PKG) primes PKA for catalytic activity in cells. *J Biol Chem* 293, 4411-4421.
- Hayashi, Y., Hsiao, E.C., Sami, S., Lancero, M., Schlieve, C.R., Nguyen, T., Yano, K., Nagahashi, A., Ikeya, M., Matsumoto, Y., *et al.* (2016). BMP-SMAD-ID promotes reprogramming to pluripotency by inhibiting p16/INK4A-dependent senescence. *Proc Natl Acad Sci U S A* 113, 13057-13062.
- Heineke, J., and Molkentin, J.D. (2006). Regulation of cardiac hypertrophy by intracellular signalling pathways. *Nat Rev Mol Cell Biol* 7, 589-600.
- Jiang, X., Bomgardner, R., Brown, J., Drew, D.L., Robitaille, A.M., Viner, R., and Huhmer, A.R. (2017). Sensitive and Accurate Quantitation of Phosphopeptides Using TMT Isobaric Labeling Technique. *J Proteome Res* 16, 4244-4252.
- Kim, C., Cheng, C.Y., Saldanha, S.A., and Taylor, S.S. (2007). PKA-I holoenzyme structure reveals a mechanism for cAMP-dependent activation. *Cell* 130, 1032-1043.
- Kushnir, A., Betzenhauser, M.J., and Marks, A.R. (2010). Ryanodine receptor studies using genetically engineered mice. *FEBS Lett* 584, 1956-1965.
- Lim, S., Hermance, N., Mudianto, T., Mustaly, H.M., Mauricio, I.P.M., Vittoria, M.A., Quinton, R.J., Howell, B.W., Cornils, H., Manning, A.L., *et al.* (2019). Identification of the kinase STK25 as an upstream activator of LATS signaling. *Nat Commun* 10, 1547.
- Liu, Y., Xia, P., Chen, J., Bandettini, W.P., Kirschner, L.S., Stratakis, C.A., and Cheng, Z. (2020). PRKAR1A deficiency impedes hypertrophy and reduces heart size. *Physiol Rep* 8, e14405.
- Marks, A.R. (2013). Calcium cycling proteins and heart failure: mechanisms and therapeutics. *J Clin Invest* 123, 46-52.
- Mootha, V.K., Lindgren, C.M., Eriksson, K.F., Subramanian, A., Sihag, S., Lehar, J., Puigserver, P., Carlsson, E., Ridderstrale, M., Laurila, E., *et al.* (2003). PGC-1alpha-responsive genes involved in oxidative phosphorylation are coordinately downregulated in human diabetes. *Nat Genet* 34, 267-273.
- Najafi, A., Sequeira, V., Kuster, D.W., and van der Velden, J. (2016). beta-adrenergic receptor signalling and its functional consequences in the diseased heart. *Eur J Clin Invest* 46, 362-374.

- Navarrete-Perea, J., Yu, Q., Gygi, S.P., and Paulo, J.A. (2018). Streamlined Tandem Mass Tag (SL-TMT) Protocol: An Efficient Strategy for Quantitative (Phospho)proteome Profiling Using Tandem Mass Tag-Synchronous Precursor Selection-MS3. *J Proteome Res* *17*, 2226-2236.
- Nerstedt, A., Cansby, E., Andersson, C.X., Laakso, M., Stancakova, A., Blucher, M., Smith, U., and Mahlapuu, M. (2012). Serine/threonine protein kinase 25 (STK25): a novel negative regulator of lipid and glucose metabolism in rodent and human skeletal muscle. *Diabetologia* *55*, 1797-1807.
- Nunez-Duran, E., Chanclon, B., Sutt, S., Real, J., Marschall, H.U., Wernstedt Asterholm, I., Cansby, E., and Mahlapuu, M. (2017). Protein kinase STK25 aggravates the severity of non-alcoholic fatty pancreas disease in mice. *J Endocrinol* *234*, 15-27.
- Olsen, J.V., Blagoev, B., Gnadt, F., Macek, B., Kumar, C., Mortensen, P., and Mann, M. (2006). Global, in vivo, and site-specific phosphorylation dynamics in signaling networks. *Cell* *127*, 635-648.
- Olsen, J.V., Vermeulen, M., Santamaria, A., Kumar, C., Miller, M.L., Jensen, L.J., Gnadt, F., Cox, J., Jensen, T.S., Nigg, E.A., *et al.* (2010). Quantitative phosphoproteomics reveals widespread full phosphorylation site occupancy during mitosis. *Sci Signal* *3*, ra3.
- Oppermann, F.S., Gnadt, F., Olsen, J.V., Hornberger, R., Greff, Z., Keri, G., Mann, M., and Daub, H. (2009). Large-scale proteomics analysis of the human kinome. *Mol Cell Proteomics* *8*, 1751-1764.
- Piacentino, V., 3rd, Weber, C.R., Chen, X., Weisser-Thomas, J., Margulies, K.B., Bers, D.M., and Houser, S.R. (2003). Cellular basis of abnormal calcium transients of failing human ventricular myocytes. *Circ Res* *92*, 651-658.
- Preisinger, C., Short, B., De Corte, V., Bruyneel, E., Haas, A., Kopajtich, R., Gettemans, J., and Barr, F.A. (2004). YSK1 is activated by the Golgi matrix protein GM130 and plays a role in cell migration through its substrate 14-3-3zeta. *J Cell Biol* *164*, 1009-1020.
- Subramanian, A., Tamayo, P., Mootha, V.K., Mukherjee, S., Ebert, B.L., Gillette, M.A., Paulovich, A., Pomeroy, S.L., Golub, T.R., Lander, E.S., *et al.* (2005). Gene set enrichment analysis: a knowledge-based approach for interpreting genome-wide expression profiles. *Proc Natl Acad Sci U S A* *102*, 15545-15550.
- Sutt, S., Cansby, E., Paul, A., Amrutkar, M., Nunez-Duran, E., Kulkarni, N.M., Stahlman, M., Boren, J., Laurencikienė, J., Howell, B.W., *et al.* (2018). STK25 regulates oxidative capacity and metabolic efficiency in adipose tissue. *J Endocrinol* *238*, 187-202.
- Tasken, K., and Aandahl, E.M. (2004). Localized effects of cAMP mediated by distinct routes of protein kinase A. *Physiol Rev* *84*, 137-167.
- Taylor, S.S., Buechler, J.A., and Yonemoto, W. (1990). cAMP-dependent protein kinase: framework for a diverse family of regulatory enzymes. *Annu Rev Biochem* *59*, 971-1005.
- Taylor, S.S., Ilouz, R., Zhang, P., and Kornev, A.P. (2012). Assembly of allosteric macromolecular switches: lessons from PKA. *Nat Rev Mol Cell Biol* *13*, 646-658.
- Tyanova, S., Temu, T., Sinitcyn, P., Carlson, A., Hein, M.Y., Geiger, T., Mann, M., and Cox, J. (2016). The Perseus computational platform for comprehensive analysis of (prote)omics data. *Nat Methods* *13*, 731-740.
- Ungerer, M., Bohm, M., Elce, J.S., Erdmann, E., and Lohse, M.J. (1993). Altered expression of beta-adrenergic receptor kinase and beta 1-adrenergic receptors in the failing human heart. *Circulation* *87*, 454-463.
- Vlahos, C.J., McDowell, S.A., and Clerk, A. (2003). Kinases as therapeutic targets for heart failure. *Nat Rev Drug Discov* *2*, 99-113.

Wang, J., Gareri, C., and Rockman, H.A. (2018). G-Protein-Coupled Receptors in Heart Disease. *Circ Res* *123*, 716-735.

Zhou, H., Di Palma, S., Preisinger, C., Peng, M., Polat, A.N., Heck, A.J., and Mohammed, S. (2013). Toward a comprehensive characterization of a human cancer cell phosphoproteome. *J Proteome Res* *12*, 260-271.

Supplementary Material

Title: STK25 inhibits PKA signaling by phosphorylating PRKAR1A

Authors: Xiaokan Zhang¹, Bryan Z. Wang^{1,2}, Michael Kim¹, Trevor R. Nash^{1,2}, Bohao Liu^{1,2}, Jenny Rao¹, Roberta Lock², Manuel Tamargo², Rajesh Kumar Soni³, John Belov¹, Eric Li¹, Gordana Vunjak-Novakovic^{1,2} and Barry Fine^{1*}

Affiliations

¹ Department of Medicine, Division of Cardiology, Columbia University Medical Center, New York, NY, USA

² Department of Biomedical Engineering, Columbia University, New York, NY, USA

³ Proteomics and Macromolecular Crystallography Shared Resource, Herbert Irving Comprehensive Cancer Center, Columbia University Irving Medical Center, New York, NY, USA

*Corresponding Author

Barry Fine MD PhD

Department of Medicine, Division of Cardiology

622 West 168th Street

PH8-405B

New York, NY 10032

Supplementary Materials:

Figures S1-S7

Table S1: *Patient characteristics of end stage heart failure samples*

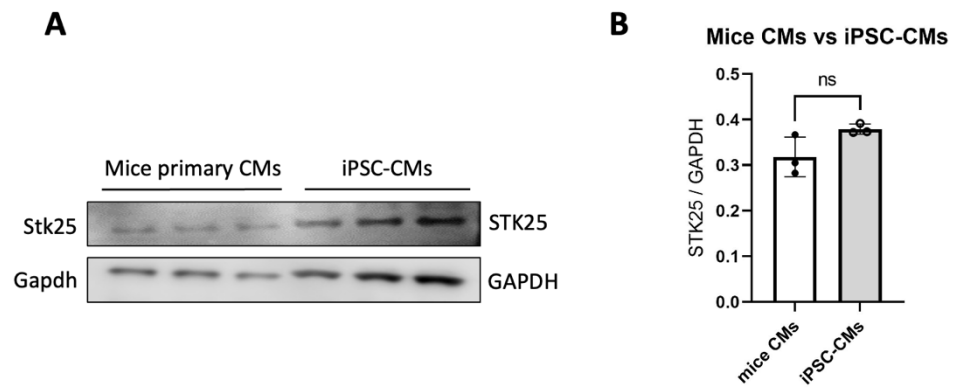


Figure S1. Comparison of STK25 expression in adult mice cardiomyocytes and in iPSC-CMs. A) Immunoblot and B) densitometry of STK25 and GAPDH expression in primary cardiomyocytes isolated from adult mouse heart and in iPSC-CMs. n=3 for each condition. Data presented as mean \pm SD, statistical significance was tested by student t-test in S1B.

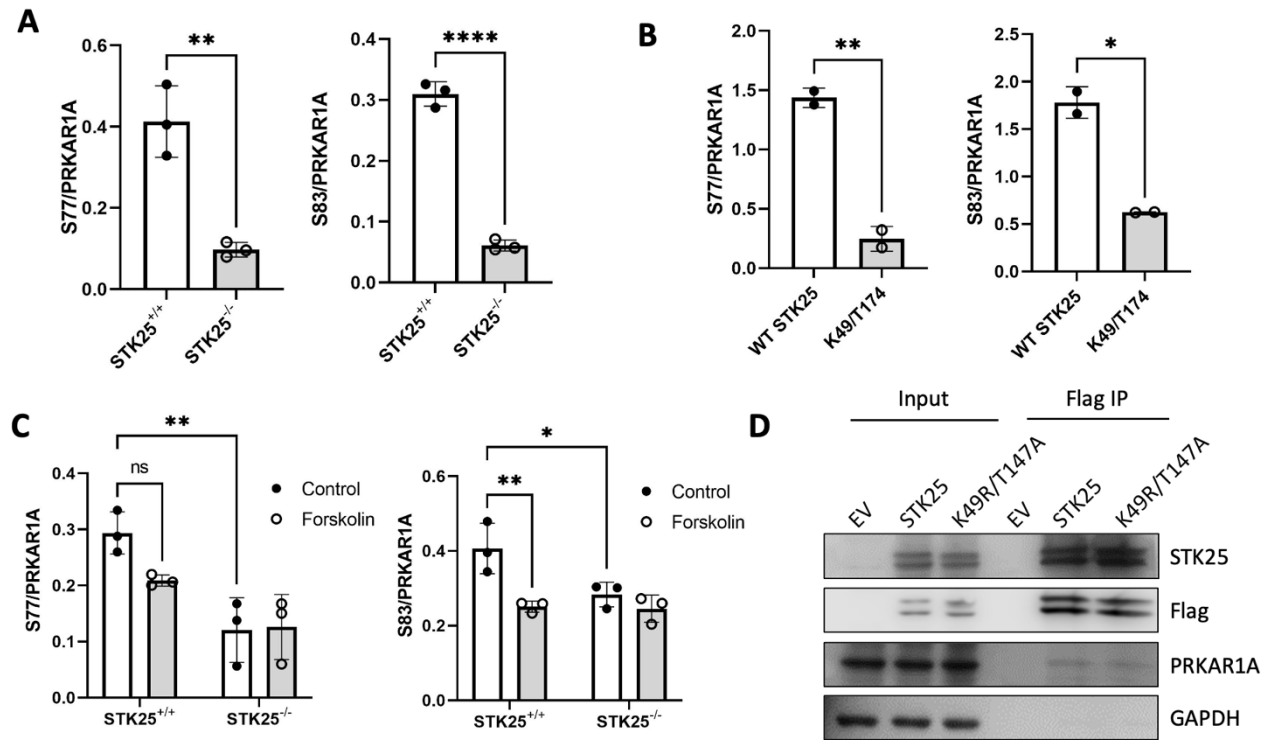


Figure S2. A) Densitometry analysis of phospho-S77 and S83 relative to total PRKAR1A in immunoblot shown in Figure 2A. B) Densitometry analysis of phospho-S77 and S83 relative to total PRKAR1A in immunoblot shown in Figure 2B. C) Densitometry analysis of phospho-S77 and S83 relative to total PRKAR1A in immunoblot shown in Figure 2C. D) Co-immunoprecipitation experiments of either wild type or kinase dead (K49R/T147A) mutant of STK25 in HEK293T cells with overexpressed flag tagged STK25 protein and endogenous PRKAR1A. For all bar graphs in this figure, n=3 for each condition, Data presented as mean +/- SD, *p<0.05, **p<0.01, and ****p<0.0001 by student's t-test in S2A and S2B and two way ANOVA with Tukey's adjustment for multiple comparisons in S2C.

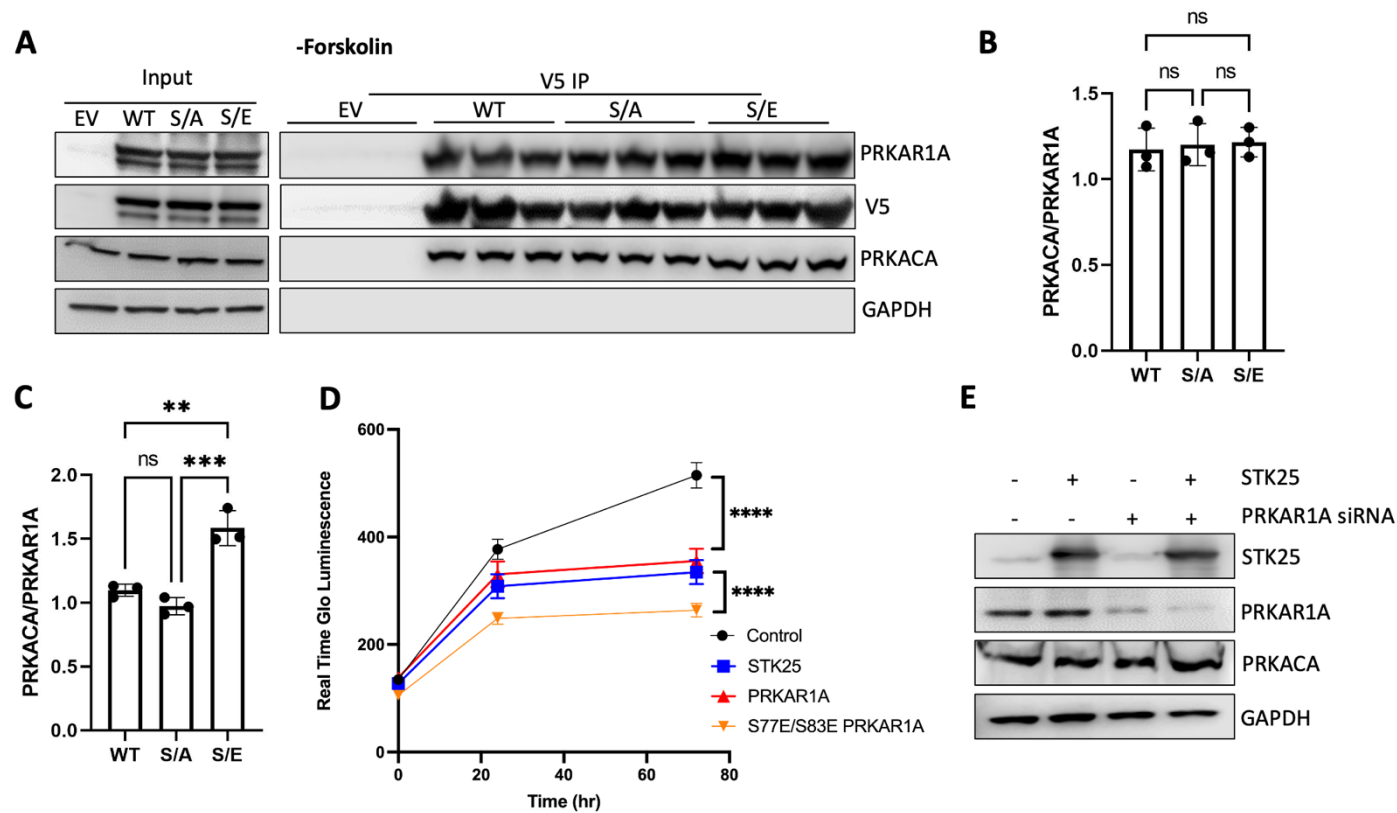


Figure S3. A) Co-immunoprecipitation of PRKAR1A-V5 with STK25 and PRKACA in HEK293T cells without forskolin treatment. B) Densitometry analysis of PRKACA relative to PRKAR1A in immunoblot shown in Figure S2A. C) Densitometry analysis of PRKACA relative to PRKAR1A in immunoblot shown in Figure 3A. D) HEK293T cells transfected with the indicated vectors and assessed for growth by Real Time Glo (Promega) over three days. E) Immunoblot demonstrating both overexpression of STK25 and knockdown of PRKAR1A in HEK293T cells shown in Figure 3D. For all graphs in this figure, n=3 for each condition or time point, Data presented as mean +/- SD, **p<0.01, ***p<0.001 and ****p<0.0001 one way ANOVA in S3A and S3C and two way ANOVA, all with Tukey's adjustment for multiple comparisons.

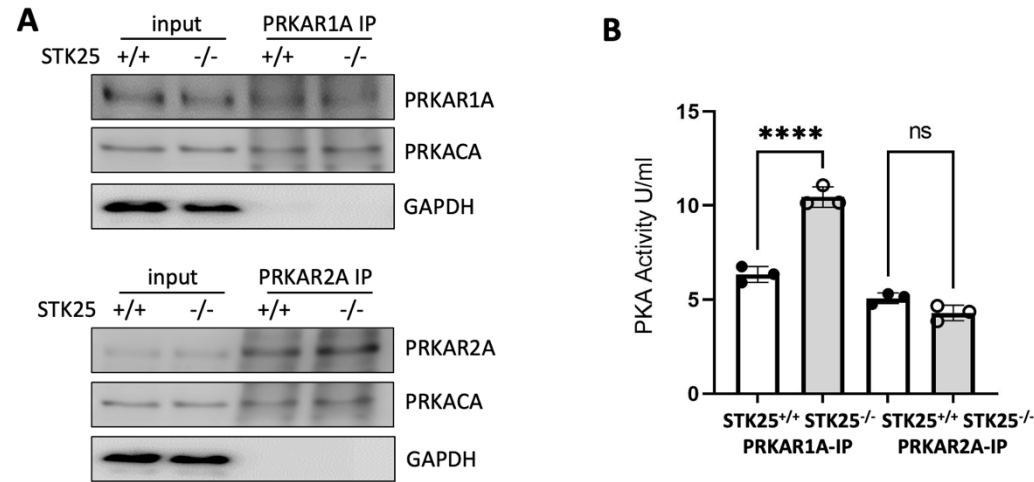


Figure S4: Comparison of Type I versus Type II holoenzyme activity in response to STK25 loss. A) Immunoprecipitations of PRKAR1A or PRKAR2A in STK25^{+/+} and STK25^{-/-} iPSC-CMs and immunoblotting for PRKAR1A or PRKAR2A, PRKACA and GAPDH. B) PKA activity of type I and II PKA holoenzymes precipitated from cell lysates of STK25^{+/+} and STK25^{-/-} iPSC-CMs. N=3 for each condition, mean +/- SD, ****p<0.0001 two way ANOVA with Sidak's adjustment for multiple comparisons.

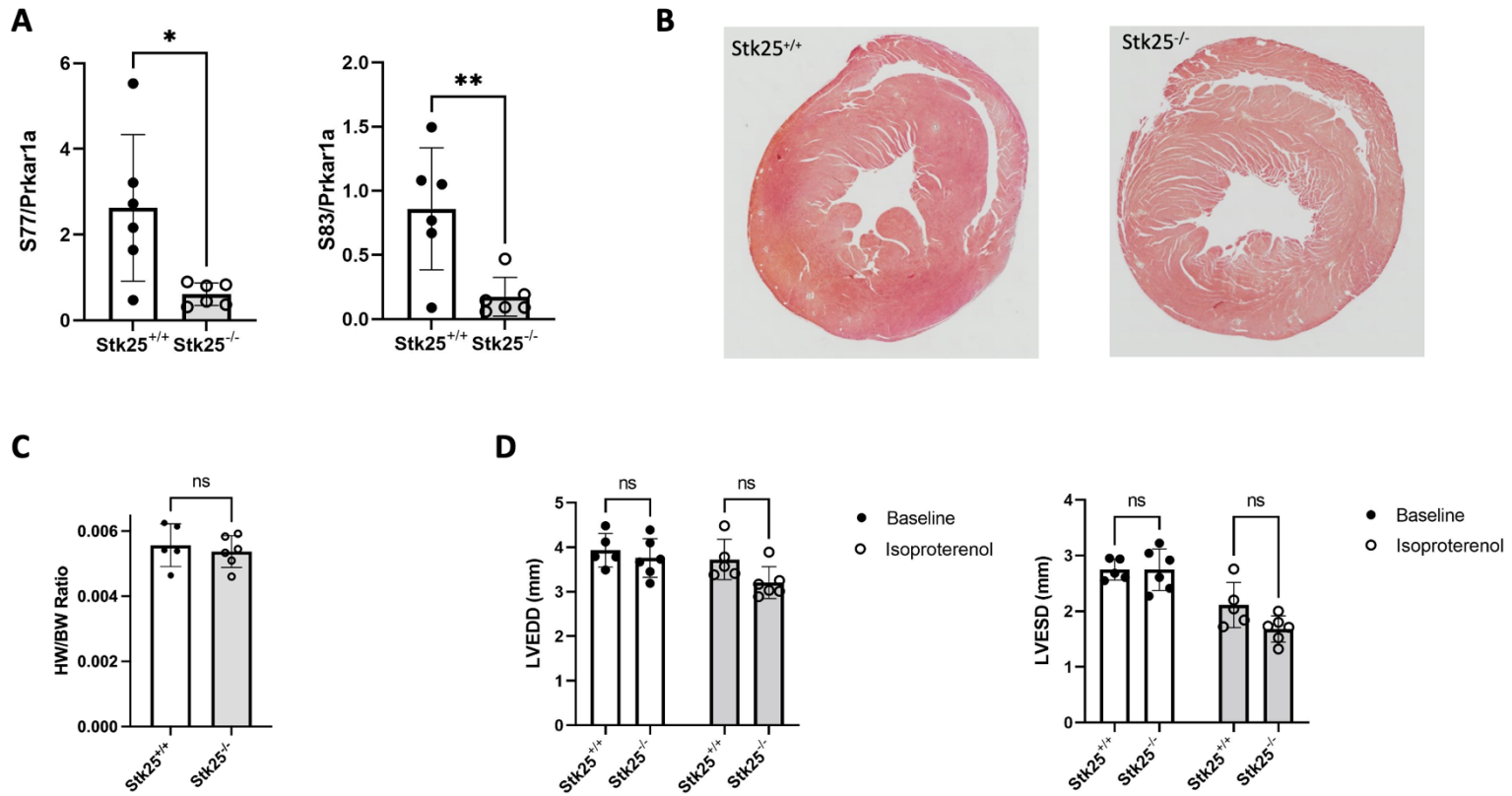


Figure S5. A) Densitometry analysis phospho-S77 and S83 relative to total Prkar1a in immunoblot shown in Figure 4A. B) Representative pentachrome staining of mid ventricle sections of 20-week old *Stk25^{+/+}* and *Stk25^{-/-}* mice. C) Heart weight (HW) to body weight (BW) ratio of mouse hearts at 20 weeks. D) Chamber measurements LVEDD (mm) and LVESD (mm) of mice at baseline and treated with isoproterenol. n=5 for *Stk25^{+/+}* and n=6 for *Stk25^{-/-}* mice. Data presented as mean +/- SD, statistical significance was tested with student's t-test in S5A, Welch's t-test in S5C, and repeated measures 2-way ANOVA with Sidak's correction for multiple comparisons in S5D.

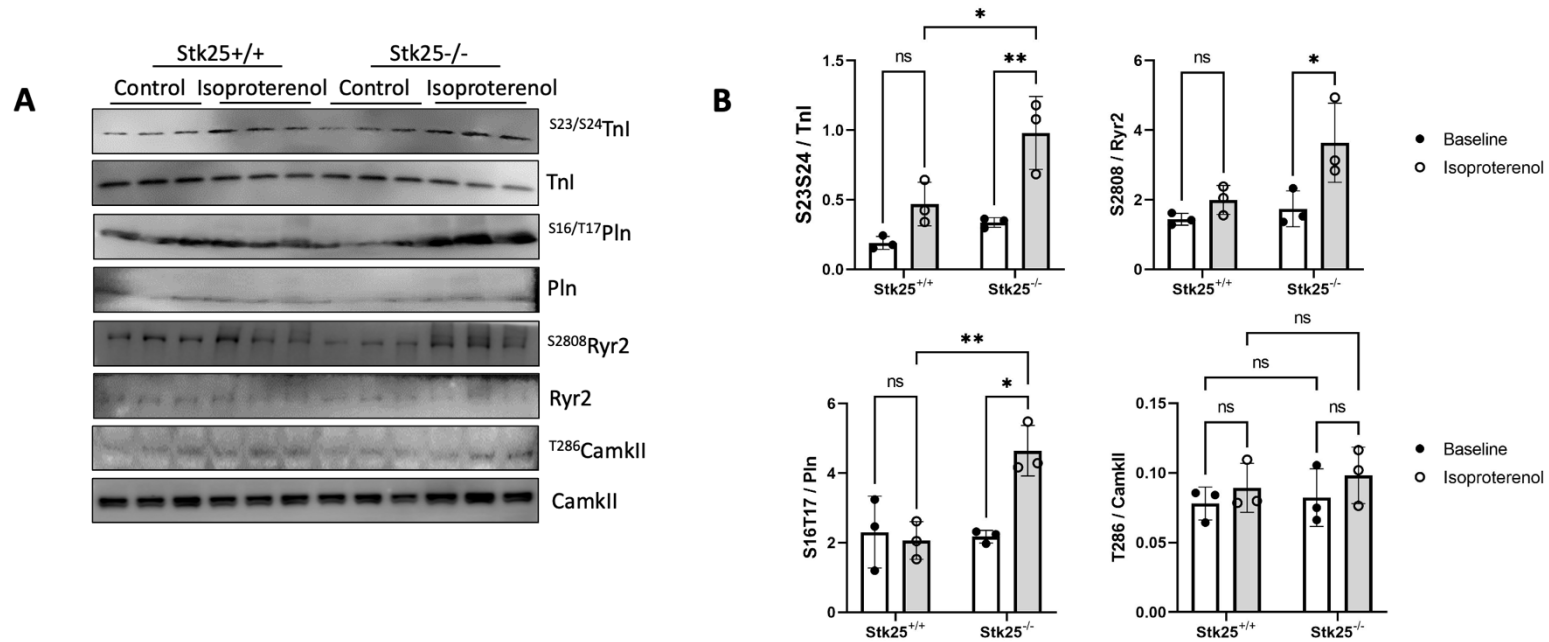


Figure S6: *Stk25* knockout and beta-adrenergic response. A) Immunoblot of phospho-S23/S24 and total Tnl, phospho-S16/T17 and total Pln, phospho-S2808 and total Ryr2, phospho-T286 and total CamkII in *Stk25*^{+/+} and *Stk25*^{-/-} whole heart lysates with and without isoproterenol injection. B) Densitometry analysis of phospho-S23/S24 relative to total Tnl, phospho-S16/T17 relative to total Pln, phospho-S2808 relative to total Ryr2, phospho-T286 relative to total CamkII in immunoblot shown in Figure S6C, n=3 for each condition. Data presented as mean +/- SD, *p<0.05, **p<0.01, statistical significance was tested with two way ANOVA with Tukey's correction for multiple comparisons.

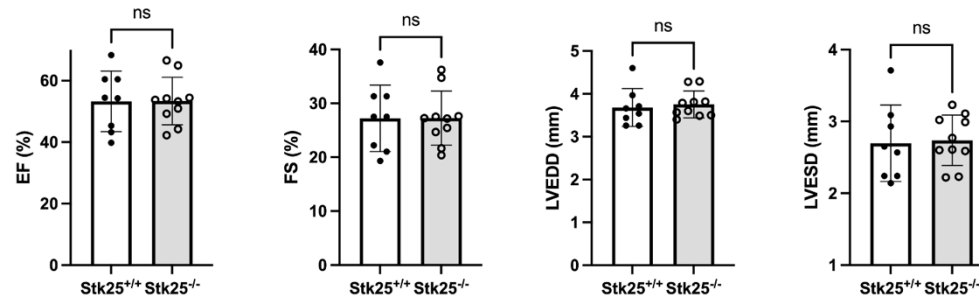


Figure S7: *Cardiac function at one year in Stk25^{-/-} mice.* Echocardiographic measurements of LV function and size in a survival cohort at 52 weeks for Stk25^{+/+} (n=8) and Stk25^{-/-} (n=10). Data presented as mean \pm SD, statistical significance was tested with a Welch's t-test.

Patient Characteristics (n=17)		
	Age (SD)	49.47 (12.8)
	Gender (Male%)	82.4
	BMI (SD)	24.4 (3.3)
Cardiomyopathy		
	Non-ischemic (%)	70.6
	Ischemic (%)	29.4
Comorbidities		
	Hypertension (%)	17.6
	Hyperlipidemia (%)	29.4
	Diabetes(%)	23.5
Heart Function		
	Ejection Fraction (%)	17.9
	LVAD	88.23
	Inotrope	35.3
Medical Therapy		
	ACEi/ARB/ARNI	29.4
	Beta Blocker	76.5
	MRA	52.9
	Anticoagulation	88.23
	Antiarrhythmic	41.2

Table S1: Patient characteristics of end stage heart failure samples

Abbreviations: SD, standard deviation; BMI, body mass index; LVAD, left ventricular assist device; ACEi, angiotensin converting enzyme inhibitor; ARB, angiotensin II receptor blocker; ARNI angiotensin II receptor blocker and neprilysin inhibitor; MRA, mineralcorticoid receptor antagonist.